JVSTB Journal of Vacuum Science & Technology B

Process and properties of the carbon nanotube assisted LiCoO 2 thin-film battery electrode by pulsed laser deposition

An-Ya Lo, Chuan-Shu Sun, Wen-Shou Tseng, and Cheng-Tzu Kuo

Citation: Journal of Vacuum Science & Technology B **27**, 3067 (2009); doi: 10.1116/1.3264678
View online: http://dx.doi.org/10.1116/1.3264678
View Table of Contents: http://scitation.aip.org/content/avs/journal/jvstb/27/6?ver=pdfcov
Published by the AVS: Science & Technology of Materials, Interfaces, and Processing

Process and properties of the carbon nanotube assisted $LiCoO_2$ thin-film battery electrode by pulsed laser deposition

An-Ya Lo, Chuan-Shu Sun, and Wen-Shou Tseng
Department of Materials Science and Engineering, National Chiao Tung University, Hsinchu 30010, Taiwan

Cheng-Tzu Kuo[a)]
Department of Materials Science and Engineering, MingDao University, Changhua 52345, Taiwan

(Received 8 July 2009; accepted 26 October 2009; published 4 December 2009)

In this study, a pulsed laser deposition process was developed to deposit a carbon nanotube (CNT) assisted $LiCoO_2$ electrode to improve its power density. The electrodes were deposited on Pt-coated Si substrates with Ar and O_2 as sputtering gases and $LiCoO_2$+C as the target. The results indicate that the working pressure is the most important parameter to control the composition of the electrode. Therefore, electrodes with a three-layer structure (i.e., $LiCoO_2$-rich/CNT-rich/$LiCoO_2$-rich) were fabricated by a three-step deposition process by varying the pressures from 13 to 1.3×10^4 Pa and then 13 Pa again, and it was found that the charge/discharge capacity became approximately 1.5 times greater than that in the corresponding electrode without a CNT-rich layer. The results also indicate that a higher substrate temperature is favorable for improving the crystallinity of the electrode to approach $LiCoO_2$ crystals. © *2009 American Vacuum Society.*
[DOI: 10.1116/1.3264678]

I. INTRODUCTION

Solid-state thin-film lithium batteries were first reported by Kanehori *et al.* in 1983; since then, considerable developments were witnessed in this area because such batteries can potentially have a long lifetime, high energy density, small self-discharge, minimal memory effect, low toxicity and safe usage, flexibility, and rechargeability.[1,2] Therefore, lithium-based batteries are the most promising candidates for miniaturized batteries for microelectronic devices and implanted biomedical cells.

Because the active materials in the electrodes of lithium batteries, such as $LiCoO_2$ and $LiMn_2O_4$, have low electronic conductivities, carbon black and graphite were utilized as conducting agents to enhance the conductivity and chemical inertness in the positive electrode (cathode).[3–5] On the other hand, carbon nanotubes (CNTs) were mechanically mixed not only to improve the properties of fuel cells and solar cells but also to improve the performance of the cathode and anode in Li-ion secondary batteries because of its excellent thermal and electronic conductivities, excellent chemical stability, and higher specific surface area.[6–11] However, these proposed processes are not suitable for fabricating CNT-assisted thin-film electrodes. In this study, we investigate the feasibility of fabricating CNT-assisted $LiCoO_2$ thin-film electrodes using a laser ablation deposition process.

II. EXPERIMENT

First, Pt-coated Si wafers were used as substrates; here, the Pt layer (thickness: 100 nm) was deposited by a duel electron-gun evaporator (ULVAC EBX-10C) under a pressure of 3.5×10^{-4} Pa, and it was used as a current collector. The substrates were then deposited by the pulsed laser deposition (PLD) method using a CO_2 laser (wavelength: 10.6 μm). The PLD target contains 91 wt % $LiCoO_2$ and 9 wt % graphite. The substrate-to-target distance is set at 3 cm. The main processing parameters include the system pressure [$(13-1.3)\times10^4$ Pa], substrate temperature (25–600 °C), and Ar/O_2 gas ratio (100/20–100/2). The specimen designations and their deposition conditions are listed in Tables I and II.

The surface morphologies, microstructure, and contents of each species of deposited films were characterized by using a JEOL JSM-6700 field-emission scanning electron microscope (SEM), JEOL JEM-2100 field-emission transmission electron microscope (TEM), and Thermo K-alpha x-ray photoelectron spectroscope (XPS), respectively. The atomic ratios of lithium and cobalt were analyzed by quantitative XPS analysis. The crystallization structures and the bonding properties of deposited films were characterized using a Siemens D-5000 x-ray diffractometer (XRD) using the detector scan mode and a Jobin Yvon LabRam HR Raman spectrometer with a wavelength of 514.5 nm (Ar laser). Finally, an HCH Instruments 604C-Electrochemical Analyzer three-electrode cyclic voltammetry (CV) measurement system was employed to survey the electrochemical properties in a potential range from −1 to 1 V with a scan rate of 50 mV/s using a Pt counter electrode, and Ag/AgCl (1*M* LiCl in MeOH) as a reference electrode in a nonaqueous 1*M* $LiClO_4$/propylene carbonate electrolyte.

III. RESULTS AND DISCUSSIONS

A. Effect of pressure on electrode compositions

Figures 1(a)–1(c) show the SEM images of the PLD-deposited films under 13, 1.3×10^3, and 1.3×10^4 Pa, respectively; it is observed that CNTs are undetectable for

[a)]Author to whom correspondence should be addressed; electronic mail: kuoct@mdu.edu.tw

TABLE I. Specimen designations, deposition conditions, and the corresponding Li/Co mole ratio by one-step process.

Specimen designation[a]	Substrate temperature (°C)	Pressure (Pa)	Ar/O_2	Lo/Co atomic ratio[b]
A1	RT	1.3×10	100/2	1.48
A2		6.5×10^2	100/2	11.8
A3		1.3×10^3	100/2	23.9
A4		1.3×10^4	100/2	393
A5		1.3×10	100/10	···
A6		1.3×10	100/20	···
B1	300	13	100/2	···
B2	400			···
B3	500			···
B4	600			···

[a]Each specimen was deposited for 2 h.
[b]Calculated by quantitative XPS.

pressures below 1.3×10^3 Pa, but they are detectable for a pressure of up to 1.3×10^4 Pa. Moreover, Fig. 1(d), which shows a TEM image of Fig. 1(c), clearly indicates the existence of multiwalled carbon nanotubes (MWCNTs) having a diameter of 10–15 nm. The pressure dependence of CNT deposition is in good agreement with previously reported results,[12] in which CNTs were produced with pressures greater than 6700 Pa by CO_2 laser ablation.

On the other hand, quantitative XPS analyses indicate that the Li/Co ratios of the electrodes are also pressure dependent; these vary from 1.5 to 393 when the pressure is varied from 13 to 1.3×10^4 Pa (shown in Table I). Such selective ablation efficiency of different elements in the target is due to the fact that it is difficult to excite elements with a higher melting temperature and atomic size using a laser beam. Thus, a lower pressure is required to approach an ideal Li/Co ratio of 1.0.

To further determine the constituents of the electrodes, four electrode films deposited under pressures of 13, 6.5×10^2, 1.3×10^3 Pa, and 1.3×10^4 Pa (specimens A1, A2, A3, and A4, respectively) were analyzed by XPS (Co $2p$). Figures 2(a) and 2(c) show XPS (Co $2p_{3/2}$,$2p_{1/2}$) and (Li $1s$) spectra, respectively, for the same four films. The decomposed spectrum for specimen A1 ($Li/Co\sim1$) is shown in Fig. 2(b), in which two sets of peaks indicate the existence of Co^{3+} and Co^{4+}.[13] Each set contains four peaks. The former set (Co^{3+}) including Co $2p_{3/2}$ (779.9 eV) and Co $2p_{1/2}$ (794.9

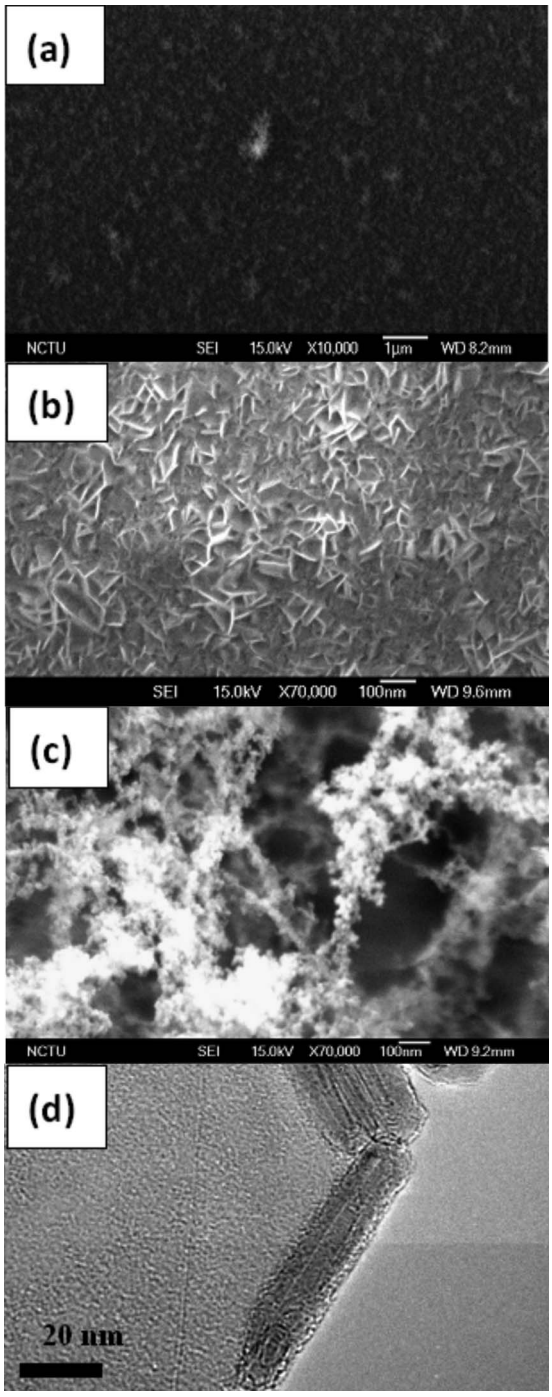

FIG. 1. SEM images of the films deposited under different pressures: (a) 13 Pa, (b) 1.3×10^3 Pa, and (c) 1.3×10^4 Pa; (d) the corresponding TEM of (c).

TABLE II. Specimen designations and deposition conditions for three-step deposition process.

	Step 1		Step 2		Step 3	
Specimen designation	Pressure (Pa) (Ar/O_2)	Temperature (°C)	Pressure (Pa) (Ar/O_2)	Temperature (°C)	Pressure (Pa) (Ar/O_2)	Temperature (°C)
D1	13(100/2)	300	1.3×10^4(100/2)	300	13(100/2)	300
D2		400		400		400
D3		500		500		500
D4		600		600		600

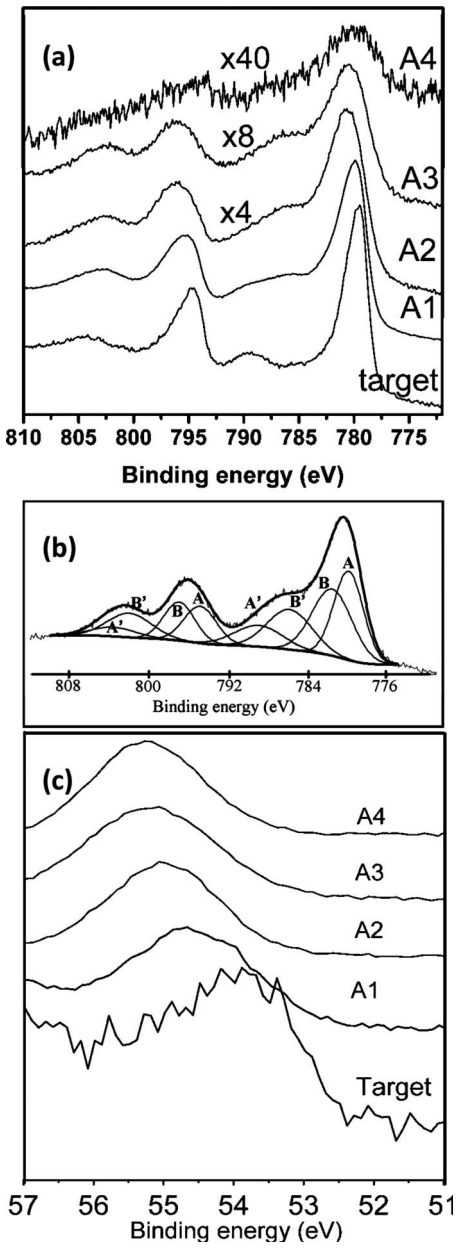

FIG. 2. XPS spectra for films deposited under three different pressures for PLD target and specimens A1–A4: (a) Co 2*p* spectra, (b) Li 1*s* spectra, and (c) decomposed spectrum for $P=13$ Pa in (a).

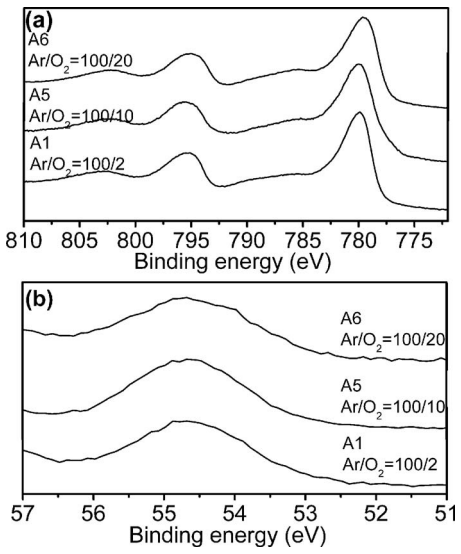

FIG. 3. XPS spectra for films deposited under different Ar/O_2 ratios for specimens A1, A5, and A6: (a) Co 2*p* spectra and (b) Li 1*s* spectra.

eV) with their respective satellite peaks at 789.0 and 803.7 eV corresponds to the existence of $LiCoO_2$. Additionally, the latter one (Co^{4+}) including Co $2p_{3/2}$ and Co $2p_{1/2}$ with their respective satellite peaks located at 781.6, 797.0, 785.9, and 802.1 eV corresponds to the existence of CoO_2. Furthermore, the cobalt ratio in the electrode films (from A1 to A4) decreases with increasing deposition pressure (13, 6.5×10^2, 1.3×10^3, and 1.3×10^4 Pa), as shown in (Co 2*p*) in Fig. 2(a) and Table I.

In addition, an important modification that should be noted is the fact that as compared to the main peak (Co 2*p*3/2 at 779.5 eV) of the PLD target, there is a significant broadening of Co 2*p*3/2 in specimens A–1A4 [shown in Fig. 2(a)], and this is rather obvious at a higher deposition pressure. This phenomenon is due to the deintercalation of lithium from $LiCoO_2$ in which a large amount of Co^{3+} ($LiCoO_2$ in target) transfers to Co^{4+} under laser ablation.[14] This statement is in agreement with the result of XPS (Li 1*s*) shown in Fig. 2(c). As compared to the XPS (Li 1*s*) peak of the target [Fig. 2(c)], it is obvious that specimen A1 shifts to a higher binding energy. Moreover, it shifts further when the deposition pressure is increased (specimens A2–A4). This indicates that lithium deintercalates from the octahedral environment of oxygen atoms ($LiCoO_2$ lattice) and forms lithium carbide (LiC_6, LiC_2, and LiC_3) (Refs. 15 and 16) during the PLD process.

In other words, the ideal Li/Co atomic ratio of 1.0 of Li_xCoO_2 for the lithium battery electrode can only be realized under a pressure less than 13 Pa by PLD, and MWCNTs can only be fabricated under a pressure of 1.3×10^4 Pa. That is, it can be realized by alternately depositing CNT-rich and Li_xCoO_2-rich layers under high and low pressures, respectively.

B. Effect of Ar/O_2 ratio on electrode compositions and substrate temperature on electrode crystallinity

Considering the effect of the Ar/O_2 ratio on the electrode compositions, specimens A1, A5, and A6 deposited under Ar/O_2 ratios of 100/2, 100/10, and 100/20 were analyzed by XPS. Figures 3(a) and 3(b) show the Co 2*p* and Li 1*s* spectra, respectively, of specimens A1, A5, and A6. These spectra show a negligible difference between Li_xCoO_2-rich electrodes deposited under difference gas ratios, suggesting that the compositions of the deposited films would not be affected by the Ar/O_2 ratio under PLD deposition at 13 Pa.

Because the main peaks of $LiCoO_2$ (Co^{3+}) and CoO_2 (Co^{4+}) are very close to each other (779.6 and 781.4 eV, respectively) in XPS but far apart in the Raman spectrum (596 and 680 cm^{-1}, respectively), the effect of deposition

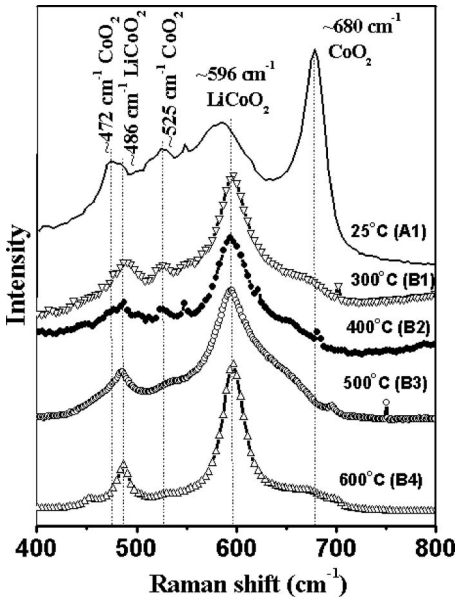

FIG. 4. Raman spectra of the electrodes deposited under low pressure (13 Pa) at different substrate temperatures.

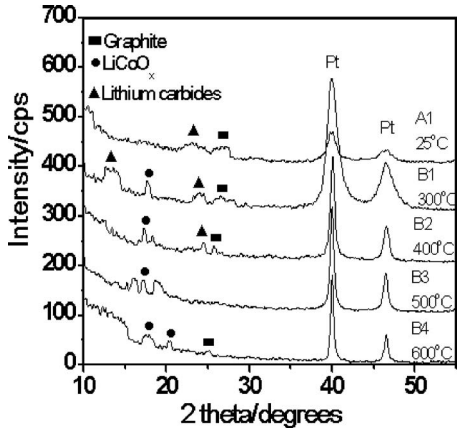

FIG. 5. XRD patterns of the electrodes deposited under low pressure (13 Pa) at different substrate temperatures for specimens with one-step deposition process.

temperature on the elimination of lithium deintercalation in the Li_xCoO_2 electrode was studied using the Raman spectrum. Figure 4 shows the Raman spectra of Li_xCoO_2-rich electrodes deposited under temperatures of 25, 300, 400, 500, and 600 °C, respectively. The Raman peaks around 486 and 596 cm^{-1} indicate the existence of $LiCoO_2$, and that at 680 cm^{-1} indicates the existence of CoO_2; this is in agreement with the XPS results. By comparing the Raman results, it is obvious that the amount of CoO_2 depends on the substrate temperature. In the case of a specimen deposited at room temperature, a large amount of CoO_2 is found in the electrode; in contrast, CoO_2 cannot be detected in a specimen deposited at 600 °C. This is consistent with a narrow full width at half maximum for $LiCoO_2$ peaks at 486 and 596 cm^{-1} at higher deposition temperatures (Fig. 4). The better crystallinity of $LiCoO_2$ at higher temperature is probably attributable to the greater probability of forming Co^{3+} at thermodynamically stable phases under a pressure of 13 Pa with an Ar/O_2 ratio of 100/2. It can be summarized that a better $LiCoO_2$ phase can be obtained by increasing the heat treatment temperature.

On the other hand, the XRD spectrum shown in Fig. 5 indicates that the amount of lithium carbides decreased and that of $LiCoO_2$ increased with an increase in the substrate temperature; this is in agreement with the Raman results.

C. High-resolution TEM of CNT-assisted electrodes

The microstructures and crystal structures of CNT-assisted composite electrodes were characterized by high-resolution TEM (HRTEM) and electron diffraction. Figure 6 shows HRTEM images of MWCNTs in the CNT-assisted composite electrode deposited at 600 °C; there exist two types of CNTs in this electrode, namely, MWCNTs with and without catalysts in the tubes with diameters of around 10–50 nm [Fig. 6(a)] and 10–15 nm [Fig. 6(b)], respectively. Figure 7 shows the HRTEM lattice image and the corresponding electron diffraction pattern of $LiCoO_2$ in the CNT-assisted electrode deposited at 600 °C, where diffractions of

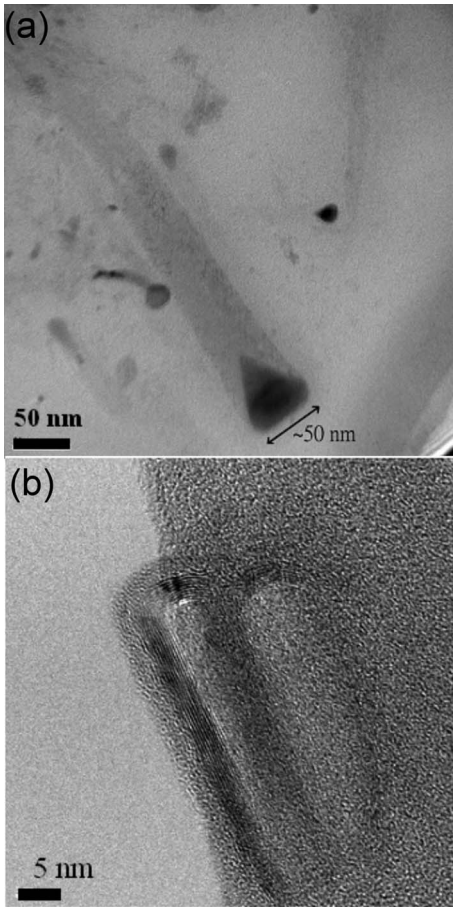

FIG. 6. TEM images of MWCNTs in specimen D4 (a) with and (b) without catalyst.

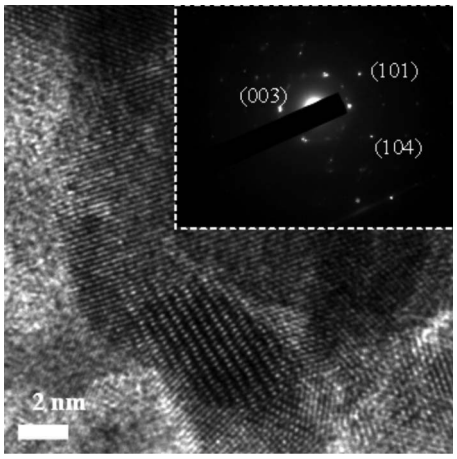

FIG. 7. HRTEM lattice image and corresponding selective area diffraction pattern of electrodes deposited by three-step deposition process.

(003), (101), and a weak (104) can be observed. In summary, the composite electrode deposited at 600 °C gives good crystallinity CNT-assisted $LiCoO_2$.

D. Electrochemical properties of CNT-assisted electrodes

The electrochemical properties of the composite electrodes and the conventional electrode are characterized by CV measurements. Figure 8 shows the CV curves (the 20th cycle) of specimens B4 and D4 for electrodes without and with CNT-rich deposition deposited at 600 °C, respectively. Both curves indicate an oxidation peak and a reduction peak indicating the charge and discharge reactions, respectively. Impurities such as lithium carbide and CoO_2 should affect the shape of the CV curves; however, it is difficult to identify them from the broadened oxidation and reduction peaks. In addition, it is clear that the CV loop area of specimen D4 is greater than that of specimen B4, suggesting that additional CNT-rich deposition leads to better electrode performance. Figures 9(a) and 9(b) show the anodic and cathodic peaks of electrodes deposited under various temperatures, respectively, in which the peak values are indexes of the charge/discharge capacity. It indicates that the values of both the anodic and cathodic peaks in the CV curve, indicating the charge discharge capacity of the electrode, increase with substrate temperature. In addition, the peak value also increases by a factor of ~1.5 with CNT-rich deposition in the electrode for electrodes deposited at 600 °C. This may be due to the fact that CNTs can create nanopores in the electrode and act as additional conductive channels for the reactions.

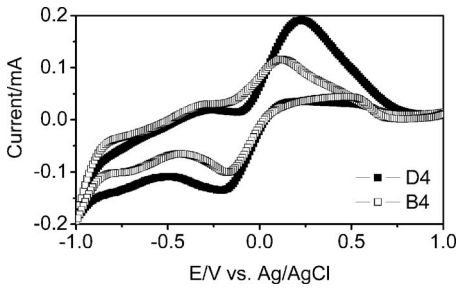

FIG. 8. CV curves (the 20th cycle) of specimens B4 and D4.

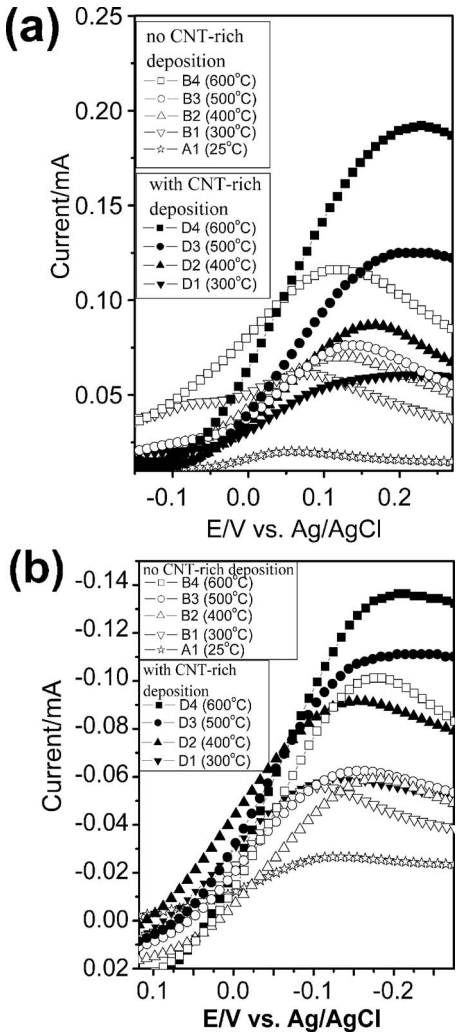

FIG. 9. CV examination results (the 20th cycle) of specimens deposited under series temperature (a) anodic peaks and (b) cathodic peaks.

IV. CONCLUSIONS

We conducted experiments to examine the fabrication process of CNT-assisted composite electrodes by PLD. It was found that a multistep process is required to prepare the composite electrode. The process includes alternately depositing CNT- and $LiCoO_2$-rich layers under high and low pressures, respectively, to create a layered structure. The results also show that the deposition temperature can increase the crystallinity of CNT-assisted $LiCoO_2$ in the composite electrodes. The CV measurements indicate that the CNT-assisted $LiCoO_2$ electrode can increase the charge/discharge capacity by a factor of 1.5 for the present sandwich-type composite electrode. We believe that further improvements can be realized by varying the percentage and types of CNTs in the composite electrode.

ACKNOWLEDGMENT

The authors would like to acknowledge the support of the National Science Council of Taiwan under Contract No. NSC 97-2221-E-451-007.

[1]M. J. J. Hack and H. Feil, U.S. Patent No. 795,018 (28 February 2001).
[2]K. Goto, T. Nakagawa, O. Nakamura, and S. Kawata, IEEE Trans. Biomed. Eng. **48**, 830 (2001).
[3]Z. Liu, J. Y. Lee, and H. J. Linder, J. Power Sources **97–98**, 361 (2001).
[4]J. K. Hong, J. H. Lee, and S. M. Oh, J. Power Sources **111**, 90 (2002).
[5]J. Kim, B. Kim, J. G. Lee, J. Cho, and B. Park, J. Power Sources **139**, 289 (2005).
[6]W. Li, C. Liang, W. Zhou, J. Qiu, Z. Zhou, G. Sun, and Q. Xin, J. Phys. Chem. **107**, 6292 (2003).
[7]R. P. Raffaelle, B. J. Landi, J. D. Harris, S. G. Bailey, and A. F. Hepp, Mater. Sci. Eng., B **116**, 233 (2005).
[8]K. Sheem, Y. H. Lee, and H. S. Lim, J. Power Sources **158**, 1425 (2006).
[9]P. Kim, L. Shi, A. Majumdar, and P. L. McEuen, Phys. Rev. Lett. **87**, 215502 (2001).
[10]Z. H. Yang and H. Q. Wu, Solid State Ionics **143**, 173 (2001).
[11]Z. H. Yang, Y. H. Zhou, S. B. Sang, Y. Feng, and H. Q. Wu, Mater. Chem. Phys. **89**, 295 (2005).
[12]M. Yudasaka, F. Kokai, K. Takahashi, R. Yamada, N. Sensui, T. Ichihashi, and S. Iijima, J. Phys. Chem. B **103**, 3576 (1999).
[13]J. C. Dupin, D. Gonbeau, H. Benqlilou-Moudden, Ph. Vinatier, and A. Levasseur, Thin Solid Films **384**, 23 (2001).
[14]L. Dahéron, R. Dedryvère, H. Martinez, M. Ménétrier, C. Denage, C. Delmas, and D. Gonbeau, Chem. Mater. **20**, 583 (2008).
[15]Y. Tao, Z. H. Chen, B. J. Zhu, and W. Z. Huang, Solid State Ionics **161**, 187 (2003).
[16]V. Z. Mordkovich, Synth. Met. **80**, 243 (1996).